

ECLIPSING BINARIES IN THE OPEN CLUSTER RUPRECHT 147. IV: THE ACTIVE TRIPLE SYSTEM EPIC 219511354

GUILLERMO TORRES¹, ANDREW VANDERBURG^{2,3}, JASON L. CURTIS⁴, ADAM L. KRAUS⁵, AND ERIC GAIDOS⁶
Accepted for publication in The Astrophysical Journal

ABSTRACT

We report follow-up spectroscopic observations of the 1.62 day, K-type, detached, active, near-circular, double-lined eclipsing binary EPIC 219511354 in the open cluster Ruprecht 147, identified previously on the basis of photometric observations from the Kepler/K2 mission. This is the fourth eclipsing system analyzed in this cluster. A combined analysis of the light curve and radial velocities yields accurate masses of $M_{\text{Aa}} = 0.912 \pm 0.013 M_{\odot}$ and $M_{\text{Ab}} = 0.822 \pm 0.010 M_{\odot}$ for the primary (star Aa) and secondary (Ab), along with radii of $R_{\text{Aa}} = 0.920 \pm 0.016 R_{\odot}$ and $R_{\text{Ab}} = 0.851 \pm 0.016 R_{\odot}$, and effective temperatures of 5035 ± 150 and 4690 ± 130 K, respectively. Comparison with current models of stellar evolution for the known age and metallicity of the cluster reveals that both radii are larger (by 10–14%) and both temperatures cooler (by $\sim 6\%$) than theoretically predicted, as is often seen in M dwarfs. This is likely caused by the significant stellar activity in the system, manifested here by 6% peak-to-peak out-of-eclipse variability, a filled-in H α line, and its detection as an X-ray source. We also find EPIC 219511354 to be a hierarchical triple system, with a low-mass tertiary in an eccentric 220 day orbit.

1. INTRODUCTION

Ruprecht 147 (NGC 6674) is a middle-aged open cluster with slightly supersolar metallicity ($[\text{Fe}/\text{H}] = +0.10$; e.g., Curtis et al. 2018), which was observed in late 2015 by NASA’s K2 mission (Campaign 7). It is remarkable in that it has no less than five eclipsing systems identified by Curtis (2016) that are detached, relatively bright, and therefore quite amenable to follow-up. In previous papers in this series we have presented the analysis of three of them: EPIC 219394517, EPIC 219568666, and EPIC 219552514 (Torres et al. 2018, 2019, 2020, hereafter Papers I, II, and III). These yielded accurate determinations of the masses, radii, and effective temperatures for the binary components that are in good agreement with stellar evolution theory. Importantly, these three systems also provided an accurate weighted mean age for Ruprecht 147 of $2.67^{+0.39}_{-0.55}$ Gyr. When combined with age determinations in other populations, Ruprecht 147 can then serve as a benchmark for studying the evolution of rotation in Sun-like stars as they spin down via magnetic braking (see Curtis et al. 2020), and even as a benchmark for the white dwarf initial-final mass relation (e.g., Marigo et al. 2020).

This paper deals with a fourth eclipsing system in Ruprecht 147, EPIC 219511354 (also known as Gaia DR2 4087847862581712768), which is a pair of detached K-type main-sequence stars with an orbital period of

1.62 days. Results from the Gaia mission confirm its membership in the cluster. Our original goal was to analyze the K2 photometry and new spectroscopic observations we have obtained, in order to provide a further check of stellar evolution theory in a cluster with known metallicity, and to add an independent age determination. Instead, we have found that the system is unsuitable for that purpose due to significant systematic discrepancies with the models, but provides instead a particularly interesting example of the effects of stellar activity on the global properties of stars with convective envelopes.

We begin by presenting the photometric, spectroscopic, and imaging observations in Section 2, where we also report the discovery that EPIC 219511354 is in fact a hierarchical triple system with an unseen low-mass outer companion. Our lightcurve analysis is presented in Section 3, followed by a determination of the absolute dimensions (masses, radii, temperatures, etc.) of the binary components in Section 4. We discuss the rotation of the components and various indicators of stellar activity in Section 5. Then in Section 6 we present a comparison of the measured properties for EPIC 219511354 against current models of stellar evolution, where we highlight the disagreements with theory stemming from the activity. A discussion of this and other issues, along with our conclusions, may be found in Section 7.

2. OBSERVATIONS

2.1. Photometry

EPIC 219511354 was observed by the Kepler spacecraft during Campaign 7 of its extended K2 mission,⁷ for a total of 83 days between 2015 October 4 and 2015 December 26. Onboard processing included co-adding the data as they were collected, to form “long-cadence” observa-

¹ Center for Astrophysics | Harvard & Smithsonian, 60 Garden St., Cambridge, MA 02138, USA; gtorres@cfa.harvard.edu

² Department of Physics and Kavli Institute for Astrophysics and Space Research, Massachusetts Institute of Technology, Cambridge, MA 02139, USA

³ Department of Astronomy, University of Wisconsin-Madison, Madison, WI 53706, USA

⁴ American Museum of Natural History, Central Park West, New York, NY, USA

⁵ Department of Astronomy, The University of Texas at Austin, Austin, TX 78712, USA

⁶ Department of Earth Sciences, University of Hawai’i at Mānoa, Honolulu, HI 96822, USA

⁷ Data release notes are available online at https://archive.stsci.edu/missions/k2/doc/drn/KSCI-19125-002_K2-DRN9_C7.pdf.

Table 1
Detrended K2 Photometry of EPIC 219511354

BJD (2,400,000+)	Residual flux (flattened)	Residual flux (not flattened)
57301.4866	0.99381119	0.99990281
57301.5070	0.99446314	0.99993898
57301.5275	0.99551235	1.00029860
57301.5479	0.99633834	1.00039691
57301.5683	0.99653720	0.99985861

Note. — K2 photometry after removal of instrumental effects and long-term drifts, and normalized by dividing by a spline fit to the out-of-eclipse observations (second column). The third column contains the same data without the normalization. (This table is available in its entirety in machine-readable form.)

tions with a 29.4 minute integration time. At end of the campaign, the data were downlinked to Earth, calibrated with pipeline routines run at the NASA Ames Research Center, and released to the public. We downloaded the pixel-level postage stamp data for EPIC 219511354 from the Mikulski Archive for Space Telescopes (MAST),⁸ and extracted lightcurves using a strategy similar to that employed in Papers I–III. In particular, we extracted lightcurves using a circular moving aperture with a 6'' radius (excluding the first day and a half when the spacecraft was thermally settling), and removed systematic artifacts caused by the K2 mission’s unstable pointing using the methods described by Vanderburg & Johnson (2014) and Vanderburg et al. (2016). After performing a first-pass systematics correction, we then refined the corrections by simultaneously fitting the shapes of the binary eclipses, the spacecraft systematics, and the intrinsic stellar variability, as described by Vanderburg et al. (2016). As shown later, out-of-eclipse stellar variability is quite obvious, and was removed for the detailed analysis below by fitting a spline function with the eclipses masked out. We then normalized the photometry by dividing this fit into the systematics-corrected data. The resulting lightcurve is shown during the eclipses in Section 3, and out of eclipse in Section 5, and is available for download in Table 1 with and without the normalization. Fifty pairs of eclipses (primary and secondary) are included within the 83 day duration of the observations.

2.2. Spectroscopy

Spectroscopic observations of EPIC 219511354 were carried out at the Center for Astrophysics between 2015 October and 2021 June, using the Tillinghast Reflector Echelle Spectrograph (TRES; Szentgyorgyi & Fűrész 2007; Fűrész 2008). This is a fiber-fed, bench-mounted instrument that is attached to the 1.5m Tillinghast reflector at the Fred L. Whipple Observatory on Mount Hopkins (Arizona, USA). We collected a total of 19 usable spectra at a resolving power of $R \approx 44,000$, which cover the wavelength region 3800–9100 Å in 51 orders. The signal-to-noise ratios in the order centered at ~ 5187 Å containing the Mg I b triplet range from 15 to 25 per resolution element of 6.8 km s⁻¹.

All our spectra display double lines. Radial velocities were measured in the order centered on the Mg I b triplet using the two-dimensional cross-correlation algorithm

TODCOR (Zucker & Mazeh 1994). Templates for each star were selected from a pre-computed library of synthetic spectra that are based on model atmospheres by R. L. Kurucz, and a line list tuned to better match the spectra of real stars (see Nordström et al. 1994; Latham et al. 2002). These templates cover a limited wavelength region of ~ 300 Å centered around 5187 Å, and are parameterized in terms of the effective temperature (T_{eff}), surface gravity ($\log g$), rotational broadening ($v \sin i$ when seen in projection) and metallicity ([Fe/H]). We adopted $\log g$ values of 4.5 for both stars, very near our final values from the analysis below. The metallicity was set to solar. This is close to the actual value measured for Ruprecht 147, which is [Fe/H] = +0.10 (Curtis et al. 2018; Bragaglia et al. 2018), and the minor difference has no impact on the velocities. We optimized the remaining parameters for the templates in the manner described by Torres et al. (2002), based on grids of cross-correlations over wide ranges in T_{eff} and $v \sin i$. While our template library has relatively course steps in temperature and $v \sin i$, we derived estimates of the actual temperatures and rotational velocities of the components by interpolation between grid points, obtaining 5310 ± 200 K and 5100 ± 200 K for the primary and secondary, along with $v \sin i$ values of 32 ± 3 and 31 ± 4 km s⁻¹, respectively. The uncertainties are based on the scatter from the individual spectra, conservatively increased to account for possible systematic errors in the models by adding 100 K and 2 km s⁻¹ in quadrature. The radial velocity determinations were made using the nearest templates in our grid, with 5250 K and 5000 K for the temperatures, and projected rotational velocities of 30 km s⁻¹ for both stars.

In a few of the spectra we noticed varying levels of contamination by moonlight. We removed this effect from the velocities by rederiving them with TRICOR, which is an extension of TODCOR to three dimensions (Zucker et al. 1995). For the third template we adopted parameters appropriate for the Sun. The final velocities are listed in Table 2. The flux ratio we obtained between the fainter secondary and the primary star is 0.53 ± 0.02 , corresponding to the mean wavelength of our observations (5187 Å).

A spectroscopic orbital solution based on these velocities gave rms residuals near 5 km s⁻¹ for both stars, which are larger than we expected from spectra of the quality we have. Examination of the residuals versus time revealed deviations from zero with a very similar pattern for the primary and secondary, strongly suggesting the presence of an unseen third star in the system. A triple-star solution assuming independent inner and outer Keplerian orbits indicates the outer orbit has a period of about 220 days, and a modest eccentricity of $e \approx 0.27$. Our observations cover 9.5 cycles of the outer orbit. The inner orbit, in turn, shows an eccentricity that is not statistically significant, given the data at hand. Hereafter we refer to the stars in the inner binary as Aa and Ab, and to the third star as B. We report the elements of the inner and outer orbits in Table 3, and present visual representations of the observations with our best-fit model in Figures 1 and 2. The inner period in this solution has been fixed to the value from the lightcurve solution described later. The rms residuals in this fit are reduced by a factor of two compared to our initial solution.

⁸ <http://archive.stsci.edu/>

Table 2

Heliocentric Radial-velocity Measurements of EPIC 219511354

HJD (2,400,000+)	RV_{Aa} (km s ⁻¹)	RV_{Ab} (km s ⁻¹)	Inner Phase	Outer Phase
57297.6914	80.20 ± 1.26	11.10 ± 2.03	0.9483	0.9307
57648.6636	-56.80 ± 1.34	140.50 ± 2.16	0.3233	0.5228
57853.9931	92.80 ± 1.82	-20.20 ± 2.94	0.9092	0.4543
57865.9773	-60.10 ± 1.35	146.50 ± 2.17	0.2975	0.5087
57885.9165	94.30 ± 1.65	-21.00 ± 2.65	0.5901	0.5991
57886.9386	-62.10 ± 1.57	150.60 ± 2.53	0.2202	0.6037
57907.9425	-52.00 ± 1.94	139.20 ± 3.12	0.1691	0.6990
57933.9168	-53.30 ± 1.77	145.80 ± 2.85	0.1823	0.8169
58004.7189	137.20 ± 1.59	-56.30 ± 2.57	0.8320	0.1380
58033.6031	121.80 ± 1.48	-47.10 ± 2.38	0.6391	0.2691
58037.6155	-24.31 ± 1.65	116.73 ± 2.65	0.1128	0.2873
58281.8504	133.60 ± 1.42	-65.80 ± 2.28	0.6840	0.3952
58300.8963	-4.70 ± 1.36	86.80 ± 2.19	0.4259	0.4816
58633.9426	151.50 ± 1.78	-62.70 ± 2.87	0.7495	0.9924
58662.8934	110.89 ± 1.98	-25.18 ± 3.18	0.5977	0.1238
59143.5896	72.30 ± 2.15	7.90 ± 3.46	0.9478	0.3044
59341.9628	-58.90 ± 1.69	157.40 ± 2.72	0.2452	0.2043
59371.8955	136.40 ± 1.65	-67.50 ± 2.65	0.6987	0.3401
59384.8673	137.00 ± 2.00	-72.20 ± 3.21	0.6959	0.3989

Note. — Orbital phases for the inner orbit (stars Aa and Ab) are counted from the reference time of primary eclipse T_0 given in Table 4, and those for the outer orbit from the time of periastron passage T_{AB} in Table 3.

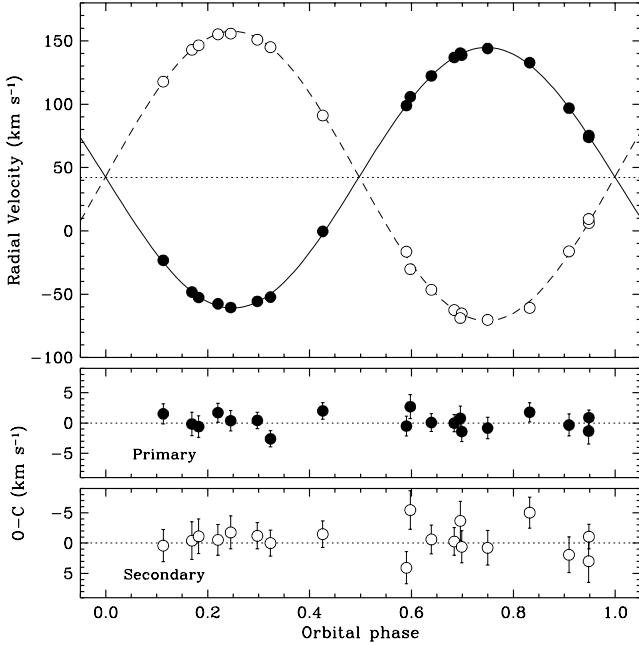


Figure 1. Radial-velocity measurements for EPIC 219511354, with our adopted model for the inner orbit (Table 3). Primary and secondary measurements are represented with filled and open circles, respectively, and have the motion in the outer orbit removed. The dotted line marks the center-of-mass velocity of the triple system. Error bars are smaller than the symbol size in the top panel, but are seen in the lower panels, which display the residuals. Phases are counted from the reference time of primary eclipse (Table 4).

We searched for the lines of the third star in our spectra using TRICOR, for observations uncontaminated by moonlight. For contaminated spectra we used QUADCOR, which is a further extension of TODCOR to four dimensions (Torres et al. 2007). No compelling sign of the tertiary was found, which we estimate we would have seen if it were any brighter than about 1% of the light of the pri-

Table 3

Spectroscopic Orbital Solution for EPIC 219511354

Parameter	Value
P_A (days)	1.6220554 (fixed)
T_0 (HJD-2,400,000)	58288.8512 ± 0.0026
γ (km s ⁻¹)	+42.57 ± 0.44
K_{Aa} (km s ⁻¹)	102.89 ± 0.57
K_{Ab} (km s ⁻¹)	114.28 ± 0.81
e_A (km s ⁻¹)	0.0068 ± 0.0050
ω_{Aa} (degree)	204 ± 34
P_{AB} (days)	220.4 ± 1.2
T_{AB} (HJD-2,400,000)	57974 ± 11
K_A (km s ⁻¹)	6.25 ± 0.81
e_{AB} (km s ⁻¹)	0.27 ± 0.11
ω_A (degree)	345 ± 21

Derived quantities

$M_{Aa} \sin^3 i$ (M_\odot)	0.906 ± 0.013
$M_{Ab} \sin^3 i$ (M_\odot)	0.816 ± 0.010
$q \equiv M_{Ab}/M_{Aa}$	0.9003 ± 0.0087
$a_{Aa} \sin i$ (10^6 km)	2.295 ± 0.013
$a_{Ab} \sin i$ (10^6 km)	2.549 ± 0.018
$a_A \sin i$ (R_\odot)	6.963 ± 0.029
$a_{AB} \sin i$ (10^6 km)	18.2 ± 2.1
$f(M)$ (M_\odot)	0.0050 ± 0.0017
$M_B \sin i / (M_{AB} + M_B)^{2/3}$ (M_\odot)	0.171 ± 0.019

Other quantities pertaining to the fit

σ_{Aa}, σ_{Ab} (km s ⁻¹)	1.62, 2.61
N_{Aa}, N_{Ab}	19, 19
Time span (days)	2087.2
Cycles covered in inner orbit	1286.7
Cycles covered in outer orbit	9.5

Note. — The symbol T_0 represents a reference time of eclipse for the inner binary; T_{AB} is a reference time of periastron passage in the outer orbit; a_{AB} is the semimajor axis of the eclipsing binary in the outer orbit; $f(M)$ is the mass function of the outer binary.

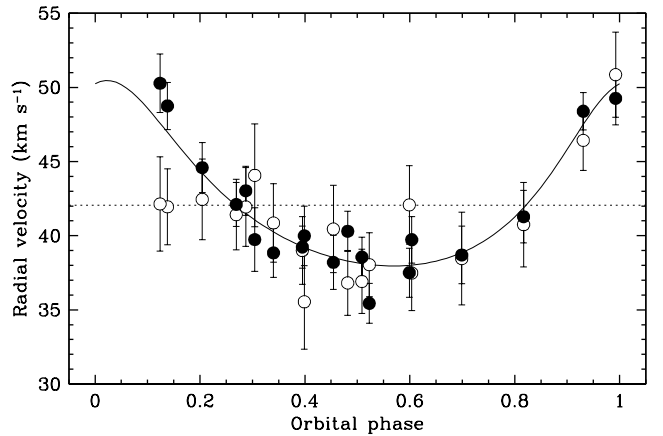


Figure 2. Radial-velocity measurements and model for EPIC 219511354 in the outer orbit, with the motion in the inner orbit removed from the measurements. Symbols and the dotted line are as in Figure 1.

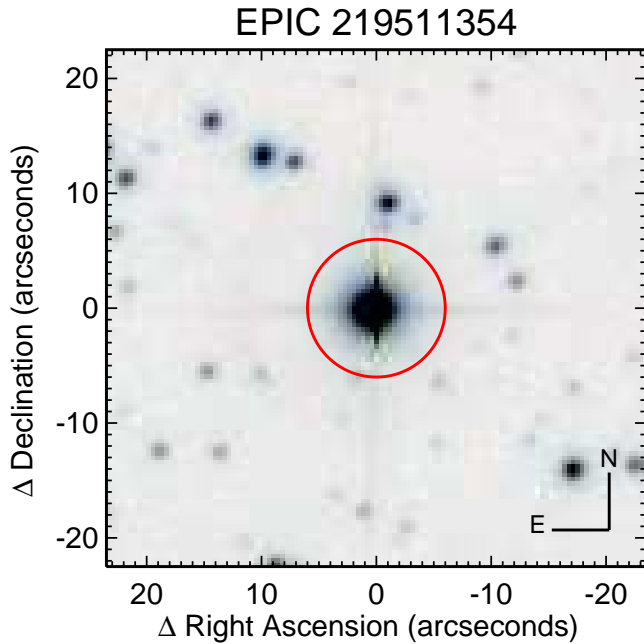


Figure 3. CFHT r -band image of the field of EPIC 219511354. The circle represents the $6''$ photometric aperture used to extract the K2 photometry.

primary star.

2.3. Imaging

Compared to a typical star in the field, membership of EPIC 219511354 in a cluster such as Ruprecht 147 carries an increased risk that objects in the vicinity may fall in the photometric aperture and affect the light curve. This does not appear to be the case here. Figure 3 shows a seeing-limited image in a band-pass similar to Sloan r (close to Kepler’s Kp band-pass), taken in 2008 by Curtis et al. (2013) with the MegaCam instrument (Hora et al. 1994) on the Canada-France-Hawaii-Telescope (CFHT). Many of the stars in this image are also listed in the Gaia EDR3 catalog (Gaia Collaboration et al. 2021), but none are inside the $6''$ radius aperture and are bright enough to have an impact.

In order to search for companions closer than seeing-limited imaging can reveal, we observed EPIC 219511354 at the Keck II Observatory with the NIRC2 infrared adaptive optics imager on UT 2016 May 12, to obtain Natural Guide Star adaptive optics imaging. We used the K' filter and followed the standard observing strategy described by Kraus et al. (2016) and previously reported for Ruprecht 147 targets by Torres et al. (2018, 2019). We obtained a short sequence of five images in vertical angle model, which stops the telescope rotator in order to allow the sky to rotate overhead and to create a uniform stellar point spread function (PSF) that enhances subsequent PSF calibration. Each image had a total integration time of 10 sec, and to avoid saturation, each image was divided into 10 exposures of 1 sec each that were coadded on the detector. The integration time allowed for four Fowler samples in each individual 1 sec exposure.

The images were analyzed using the methods described by Kraus et al. (2016). To briefly summarize, for each image the PSF of the primary star was subtracted us-

ing two methods: an azimuthal-median profile, and an empirical PSF calibrator that most closely matches the science target, chosen from among the 1000 most contemporaneous images of other stars that appeared to be single. Within each residual image, the flux as a function of position was measured in apertures of radius 40 mas, centered on each pixel, and the noise was estimated from the RMS of fluxes within concentric rings around the primary star. Finally, the detections and detection limits were estimated from the strehl-weighted sum of the detection significances in the image stack, and any location with a total significance of $> 6\sigma$ was visually inspected to determine if it was a residual speckle or cosmic ray.

We ultimately determined that there are two faint sources that share the NIRC2 field of view with EPIC 219511354, one close to the star ($\rho = 1303.1 \pm 1.9$ mas, $\theta = 189^\circ.13 \pm 0^\circ.8$, $\Delta K' = 7.024 \pm 0.024$ mag), and one much farther away ($\rho = 8383 \pm 5$ mas, $\theta = 156^\circ.17 \pm 0^\circ.03$, $\Delta K' = 8.30 \pm 0.08$ mag) that is outside the $6''$ photometric aperture. With only a single epoch, we are unable to determine if either is comoving, but given their faintness, they should not significantly bias the fitting of the light curves. The corresponding limits on additional companions were $\Delta K' = 5.5$ mag at $\rho = 150$ mas, $\Delta K' = 8.1$ mag at $\rho = 500$ mas, and $\Delta K' = 8.8$ mag at $\rho > 1''.5$.

3. LIGHTCURVE ANALYSIS

The Kepler/K2 light curve of EPIC 219511354 was analyzed in the same way as previous papers in this series, using the Nelson-Davis-Etzel binary model (Etzel 1981; Popper & Etzel 1981), which is appropriate for well-detached systems such as this in which the stars are essentially spherical (see below). Specifically, we used the implementation of this model in the `eb` code of Irwin et al. (2011), which facilitates its use within a Markov chain Monte Carlo (MCMC) environment.

The adjustable parameters we considered are the orbital period of the inner binary (P_A), a reference time of primary eclipse (T_0), the central surface brightness ratio in the Kepler band ($J \equiv J_{Ab}/J_{Aa}$), the sum of the relative radii normalized by the semimajor axis ($r_{Aa} + r_{Ab}$) and their ratio ($k \equiv r_{Ab}/r_{Aa}$), the cosine of the inclination angle ($\cos i$), the eccentricity parameters $\sqrt{e_A} \cos \omega_{Aa}$ and $\sqrt{e_A} \sin \omega_{Aa}$, where e_A is the inner binary eccentricity and ω_{Aa} the argument of periastron for the primary, and an out-of-eclipse brightness level in magnitude units (m_0). We adopted a linear limb-darkening law with fixed coefficients for the Kepler band taken from Claret & Bloemen (2011), as tests with a quadratic law gave no improvement and did not change the geometric parameters. The coefficients were interpolated in the tabulation from those authors based on the effective temperatures and surface gravities for the components described in Section 4 below, and the metallicity of $[\text{Fe}/\text{H}] = +0.10$ for Ruprecht 147. The coefficients are 0.681 for the primary and 0.717 for the secondary. As a final free parameter we included a multiplicative scale factor for the observational errors, which we assumed initially to have the same (arbitrary) value of 0.002 mag for all epochs.

Because the normalization of the light curve described in Section 2.1 artificially removes any variations out of eclipse, gravity darkening and reflection become irrele-

vant. For consistency, we therefore used the option in the `eb` code that suppresses those effects in calculating the binary model. As the out-of-eclipse portions of the light curve then provide no additional information, we retained for the analysis only sections within 0.12 in phase units from each eclipse, equivalent to about one and a half times the total eclipse duration. Third light was set to zero given the absence of any nearby companions within the photometric aperture, and the non-detection of the tertiary in our spectra. Tests with third light set to the maximum allowed by the spectroscopy resulted in only very small changes in some of the geometric parameters that are well within our final uncertainties described below.

In eclipsing binaries such as EPIC 219511354 with partial eclipses and similar components, the radius ratio k is often strongly correlated with other properties such as J , and as a result it can be poorly constrained by the photometry. This problem can be alleviated by requiring the solution to be consistent with an independently measured light ratio, such as from spectroscopy (see, e.g., Andersen et al. 1980). This is effective because the light ratio depends very strongly on the radius ratio: $\ell_{\text{Ab}}/\ell_{\text{Aa}} \propto k^2$. For this we used our measurement from Section 2.2, which we transformed to the Kepler band using synthetic spectra based on PHOENIX models from Husser et al. (2013), for the properties of the components reported below. We applied this constraint ($\ell_{\text{Ab}}/\ell_{\text{Aa}} = 0.62 \pm 0.03$) in the form of a Gaussian prior.

The cadence of the Kepler observations (29.4 minutes) is a non-negligible fraction of the orbital period of the inner binary (1.62 days), equivalent to almost 0.013 in phase units. In order to avoid biases from smearing, we oversampled the model light curve at each iteration of our solution, and then integrated over the 29.4 minute duration of each cadence prior to the comparison with the observations (see Gilliland et al. 2010; Kipping 2010). In principle, an additional bias may come from the finite light travel time of the binary in the outer orbit, advancing or delaying the times of eclipse. However, the effect is very small in this case, ranging from +0.5 minutes -1.0 minutes over the 81 days of photometric coverage. Nevertheless, we chose to apply these corrections to the individual times of observation, which we derived from our spectroscopic orbital solution.

We carried out our lightcurve analysis using the `emcee`⁹ code of Foreman-Mackey et al. (2013), which is a Python implementation of the affine-invariant MCMC ensemble sampler proposed by Goodman & Weare (2010). We used 100 walkers with chain lengths of 5,000 each, after discarding the burn-in. All parameters used uniform or log-uniform priors over suitable ranges listed in Table 4. We verified convergence by visual examination of the chains, and by requiring a Gelman-Rubin statistic of 1.05 or smaller for each parameter (Gelman & Rubin 1992). The results are reported in Table 4. The posterior distributions of the derived quantities in the bottom section of the table were constructed directly from the MCMC chains of the adjustable parameters involved. The eccentricity of the orbit is formally significant at about the 4.3σ level. The oblateness of the stars, calculated as prescribed by Binnendijk (1960), is 0.003,

⁹ <https://github.com/dfm/emcee>

Table 4
Results from our MCMC Lightcurve Analysis of EPIC 219511354

Parameter	Value	Prior
P_A (days)	$1.6220554^{+0.0000011}_{-0.0000011}$	[1.6, 1.7]
T_0 (HJD-2,400,000)	$57336.706796^{+0.000019}_{-0.000019}$	[57336, 57337]
J	$0.70167^{+0.00079}_{-0.00073}$	[0.4, 1.0]
$r_{\text{Aa}} + r_{\text{Ab}}$	$0.25377^{+0.00021}_{-0.00021}$	[0.01, 0.50]
$k \equiv r_{\text{Ab}}/r_{\text{Aa}}$	$0.924^{+0.013}_{-0.013}$	[0.5, 1.5]
$\cos i$	$0.06665^{+0.00062}_{-0.00067}$	[0, 1]
$\sqrt{e_A} \cos \omega_{\text{Aa}}$	$+0.00213^{+0.00059}_{-0.00051}$	[-1, 1]
$\sqrt{e_A} \sin \omega_{\text{Aa}}$	$-0.0682^{+0.0082}_{-0.0075}$	[-1, 1]
m_0 (mag)	$12.811994^{+0.000082}_{-0.000081}$	[12, 13]
f_{K2}	$1.439^{+0.024}_{-0.024}$	[-5, 5]
Derived quantities		
r_{Aa}	$0.13190^{+0.00082}_{-0.00082}$...
r_{Ab}	$0.12187^{+0.00093}_{-0.00092}$...
i (degree)	$86.178^{+0.038}_{-0.036}$...
e_A	$0.0047^{+0.0011}_{-0.0011}$...
ω_{Aa} (degree)	$271.78^{+0.68}_{-0.49}$...
$\ell_{\text{Ab}}/\ell_{\text{Aa}}$	$0.590^{+0.016}_{-0.016}$	$G(0.62, 0.03)$
J_{ave}	$0.69102^{+0.00078}_{-0.00072}$...

Note. — The values listed correspond to the mode of the respective posterior distributions, and the uncertainties represent the 68.3% credible intervals. Priors in square brackets are uniform over the specified ranges, except the one for f_{K2} , which is log-uniform, and the one for the light ratio, which is Gaussian, indicated above as $G(\text{mean}, \sigma)$.

which is well below the upper limit of 0.04 considered safe for the Nelson-Davis-Etzel binary model (see, e.g., Popper & Etzel 1981), justifying its use. Figure 4 shows the K2 observations together with our model.

There is significant scatter in the residuals within both eclipses (larger in the secondary), which we interpret as being caused by the presence of spots on both stars. This is consistent with other evidence of stellar activity such as the variability out of eclipse, described later. This extra scatter, which represents correlated (“red”) noise, raises the concern that it may be biasing the solution, and causing the uncertainties to be underestimated.

To address this concern, we reanalyzed the data using the complete light curve for EPIC 219511354, with the instrumental effects removed but without normalizing it by the spline fit indicated in Section 2.1, i.e., preserving the out-of-eclipse variability. We divided the data set into 25 segments, each containing two primary and two secondary eclipses, and performed independent solutions in each segment. To account for the distortions caused by spots, we added a four-term Fourier series to the model (nine extra parameters). The period was kept fixed at the value from Table 4, and the mass ratio was held at its value in Table 3. Reflection effects were modeled by solving for the albedo coefficients for each component ($A_{\text{Aa}}, A_{\text{Ab}}$), with loose Gaussian priors set to average values of 0.5, as appropriate for stars with convective envelopes, and a standard deviation of 0.3.

The median value for each parameter over the 25 seg-

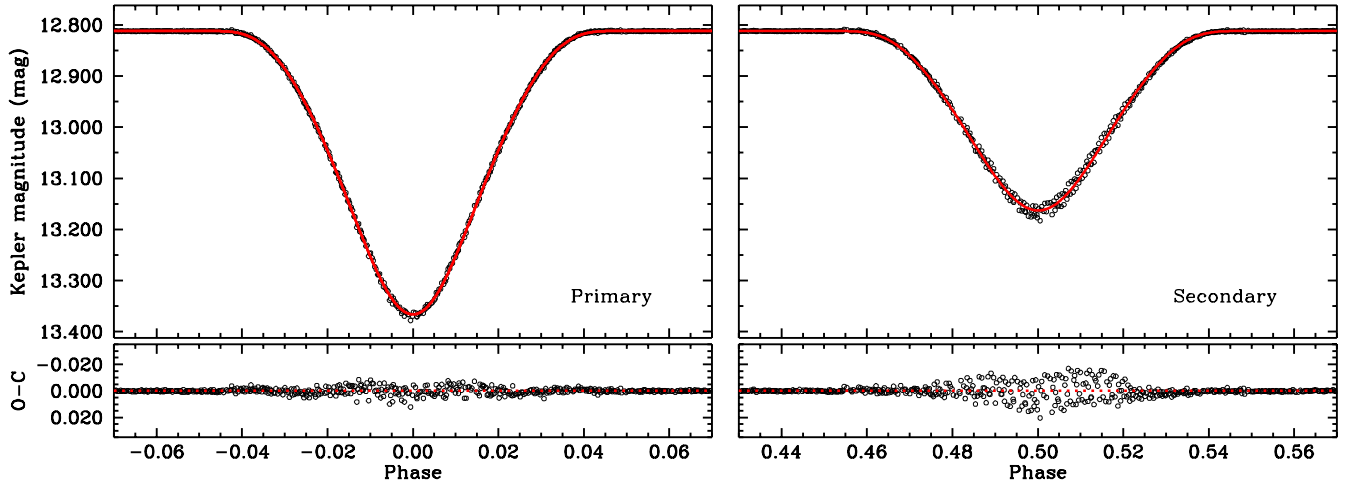


Figure 4. K2 observations and model light curve for EPIC 219511354 during primary and secondary eclipse.

Table 5

Results of Independent MCMC Analyses for 25 Segments of EPIC 219511354 Photometry, with the Addition of a 4-term Fourier Series to the Model

Parameter	Value
J	$0.693^{+0.020}_{-0.010}$
$r_{Aa} + r_{Ab}$	$0.25335^{+0.00044}_{-0.00100}$
k	$0.942^{+0.036}_{-0.023}$
$\cos i$	$0.0674^{+0.0018}_{-0.0032}$
$\sqrt{e} \cos \omega_{Aa}$	$+0.0021^{+0.0050}_{-0.0056}$
$\sqrt{e} \sin \omega_{Aa}$	$-0.074^{+0.015}_{-0.017}$
A_{Aa}	$0.422^{+0.084}_{-0.086}$
A_{Ab}	$0.26^{+0.18}_{-0.18}$
f_{K2}	$0.51^{+0.14}_{-0.12}$
Derived quantities	
r_1	$0.1307^{+0.0017}_{-0.0022}$
r_2	$0.1234^{+0.0029}_{-0.0013}$
i (degree)	$86.14^{+0.16}_{-0.11}$
e_A	$0.0052^{+0.0047}_{-0.0027}$
ω_{Aa} (degree)	$271.6^{+4.0}_{-3.5}$
ℓ_{Ab}/ℓ_{Aa}	$0.595^{+0.039}_{-0.044}$
J_{ave}	$0.683^{+0.020}_{-0.009}$

Note. — The values listed correspond to the median of the independent results for the 25 segments of the light curve, with the corresponding 68.3% confidence levels.

ments, and the corresponding 68.3% confidence intervals from the dispersion of the 25 solutions, are given in Table 5. The agreement with the results in Table 4 is excellent, suggesting our initial solution is unbiased. The uncertainties, however, are considerably larger. We have chosen to adopt these more conservative errors here, and assign them to the parameter values in Table 4. We note that the eccentricity in Table 5 appears much less significant than before. It is now different from zero at just under the 2σ level.

4. ABSOLUTE DIMENSIONS

We report the physical properties of the EPIC 219511354 components in Table 6. The masses have fractional errors of 1.4 and 1.2% for the primary and secondary, and the radii are good to about 1.8% for both stars. The measured $v \sin i$ values are both marginally larger than those predicted assuming spin-orbit synchronization and alignment for a circular orbit (v_{sync} in the table), although the difference may not be significant.

The spectroscopic temperatures in Section 2.2 are not precise enough for a useful comparison with models. In particular, the temperature difference is essentially unconstrained due to the large errors. A much more precise and accurate measure of the temperature ratio (or difference) can be obtained directly from the light curve analysis, through the surface brightness ratio J (or the disk-integrated value J_{ave} ; see Table 5). Additionally, a luminosity-weighted mean temperature can be derived from available brightness measurements for EPIC 219511354. These two quantities together allow us to infer the individual T_{eff} values.

Brightness measurements were gathered from the literature in the Johnson, Sloan, and 2MASS photometric systems (Henden et al. 2015; Skrutskie et al. 2006). We constructed nine non-independent color indices, and used color-temperature calibrations from Casagrande et al. (2010) and Huang et al. (2015) to infer the mean temperature, setting the metallicity to the known value for the parent cluster. We adopted a reddening of $E(B - V) = 0.12 \pm 0.03$, which is the average of our independent determinations for three other eclipsing binaries in Ruprecht 147 (Papers I, II, and III). A systematic difference of about 130 K exists between the temperatures inferred from the above two calibrations (see Huang et al. 2015). For consistency with our earlier studies, we adjusted the results from the Casagrande calibration to place them on the Huang zero point, and then averaged all individual values. The result is a mean system temperature of 4900 ± 100 K.

The temperature difference we obtained from the disk-integrated surface brightness ratio J_{ave} is 345 ± 60 K. The mean system temperature then leads to individual values of 5035 ± 150 K for the primary and 4690 ± 130 K for the secondary. They correspond to spectral types of K2 and K4. We list these results in Table 6.

Table 6
Physical Properties of EPIC 219511354

Parameter	Primary	Secondary
$M (M_{\odot}^N)$	0.912 ± 0.013	0.822 ± 0.010
$R (R_{\odot}^N)$	0.920 ± 0.016	0.851 ± 0.016
$\log g$ (dex)	4.470 ± 0.016	4.494 ± 0.017
$q \equiv M_2/M_1$	0.9003 ± 0.0087	
$a (R_{\odot}^N)$	6.979 ± 0.052	
T_{eff} (K)	5035 ± 150	4690 ± 130
ΔT_{eff} (K)	345 ± 60	
$L (L_{\odot})$	0.490 ± 0.060	0.316 ± 0.038
M_{bol} (mag)	5.51 ± 0.13	5.98 ± 0.13
BC_V (mag)	-0.29 ± 0.12	-0.47 ± 0.13
M_V (mag)	5.80 ± 0.22	6.46 ± 0.24
$v_{\text{sync}} \sin i$ (km s $^{-1}$) ^a	28.6 ± 0.5	26.5 ± 0.5
$v \sin i$ (km s $^{-1}$) ^b	32 ± 3	31 ± 4
$E(B - V)$ (mag)	0.12 ± 0.03	
A_V (mag)	0.372 ± 0.093	
Distance modulus (mag)	7.32 ± 0.23	
Distance (pc)	290 ± 30	
π (mas)	3.44 ± 0.37	
$\pi_{\text{Gaia/EDR3}}$ (mas) ^c	3.479 ± 0.022	

Note. — The masses, radii, and semimajor axis a are expressed in units of the nominal solar mass and radius (M_{\odot}^N , R_{\odot}^N) as recommended by 2015 IAU Resolution B3 (see Prša et al. 2016), and the adopted solar temperature is 5772 K (2015 IAU Resolution B2). Bolometric corrections are from the work of Flower (1996), with conservative uncertainties of 0.1 mag, and the bolometric magnitude adopted for the Sun appropriate for this BC_V scale is $M_{\text{bol}}^{\odot} = 4.732$ (see Torres 2010). See text for the source of the reddening. For the apparent visual magnitude of EPIC 219511354 out of eclipse we used $V = 13.013 \pm 0.029$ (Henden et al. 2015).

^a Synchronous projected rotational velocity assuming a circular orbit and spin-orbit alignment.

^b Measured projected rotational velocities.

^c A parallax zero-point correction of +0.022 mas has been added to the catalog parallax (Lindgren et al. 2021).

The luminosities together with bolometric corrections from Flower (1996) (see also Torres 2010) and an adopted visual magnitude of $V = 13.013 \pm 0.029$ (Henden et al. 2015) lead to a distance of 290 ± 30 pc, corresponding to a parallax of 3.44 ± 0.37 mas. This is in excellent agreement with the parallax listed in the Gaia EDR3 catalog (3.479 ± 0.022 mas, after corrections for a zero-point bias following Lindgren et al. 2021), and supports the accuracy of our radius and temperature determinations.

With our mass estimates for the binary components and the spectroscopic solution for the outer orbit of the triple system, we calculate a minimum mass for the tertiary of $0.27 M_{\odot}$ for an edge-on orbit. If it is a main-sequence star, the upper limit on its brightness, transformed to the Kp band, corresponds to approximately 2% of the flux of the primary star. Appealing to an isochrone for the cluster from the PARSEC 1.2S series of Chen et al. (2014), with $[\text{Fe}/\text{H}] = +0.10$ and an age of 2.67 Gyr as determined from Papers I–III, this relative flux leads to a maximum tertiary mass of about $0.47 M_{\odot}$. This places a lower limit on the inclination angle of the outer orbit of $\sim 38^{\circ}$ relative to the line of sight. However, it is also possible that the tertiary is a

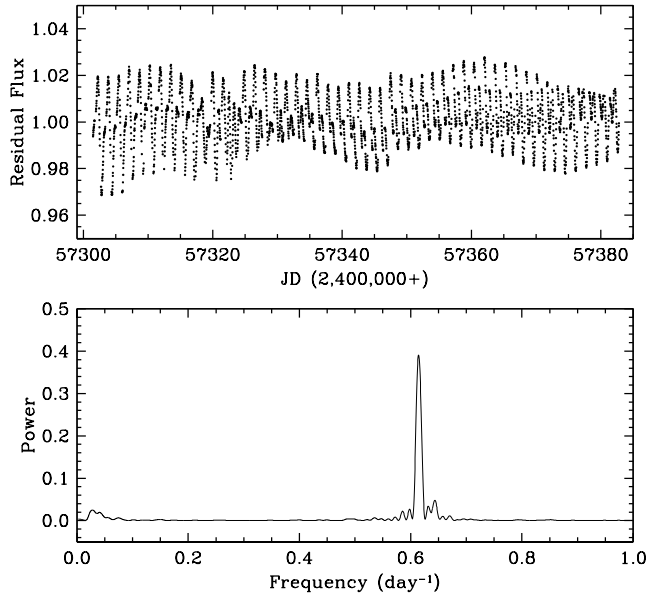


Figure 5. *Top:* Out-of-eclipse variability in the K2 photometry of EPIC 219511354, interpreted here as due to rotational modulation by spots on one or both stars. The binary eclipses have been masked out. *Bottom:* Lomb-Scargle periodogram featuring a peak at a frequency corresponding to a rotational period of $1.628^{+0.014}_{-0.017}$ days, similar to the orbital period.

more massive white dwarf. This alternative scenario will be discussed below.

5. ROTATION AND ACTIVITY

The light curve of EPIC 219511354 displays obvious variability out of eclipse that we interpret as a signature of rotation (Figure 5, top panel). The peak-to-peak amplitude over the entire 81-day time series is almost 6%, indicating a significant level of activity. The Lomb-Scargle periodogram in the lower panel displays a main peak at a frequency corresponding to $P_{\text{rot}} = 1.628^{+0.014}_{-0.017}$ days, where the uncertainty was calculated from the half width of the peak at half maximum. This period is consistent with the orbital period, within the uncertainties, suggesting spin-orbit synchronization.

The rotational modulation appears quite complex. Closer inspection reveals the presence of two distinct signals with slightly different periods. The two signals are marked with dotted and dashed lines in Figure 6, which is an enlargement of a section of the top panel of the previous figure. For each signal the intervals between consecutive maxima in the light curve were determined by eye, and are not quite the same: one signal (dotted lines) has a periodicity of 1.617 days, while the other (dashed) repeats every 1.612 days. We estimate the uncertainty in each of these estimates to be about 0.002 days. Both periods are formally consistent with the one measured from the periodogram in Figure 5, which has a larger uncertainty, and they both appear to be marginally shorter than the orbital period of 1.622 days. The individual amplitudes of the signals are difficult to pin down, and seem to vary with time.

It is unclear whether the signals correspond to different components, or to only one of the stars. The latter scenario could result from two spots or spot regions at different latitudes (and longitudes) on the same star, carried around at slightly different speeds due to differential

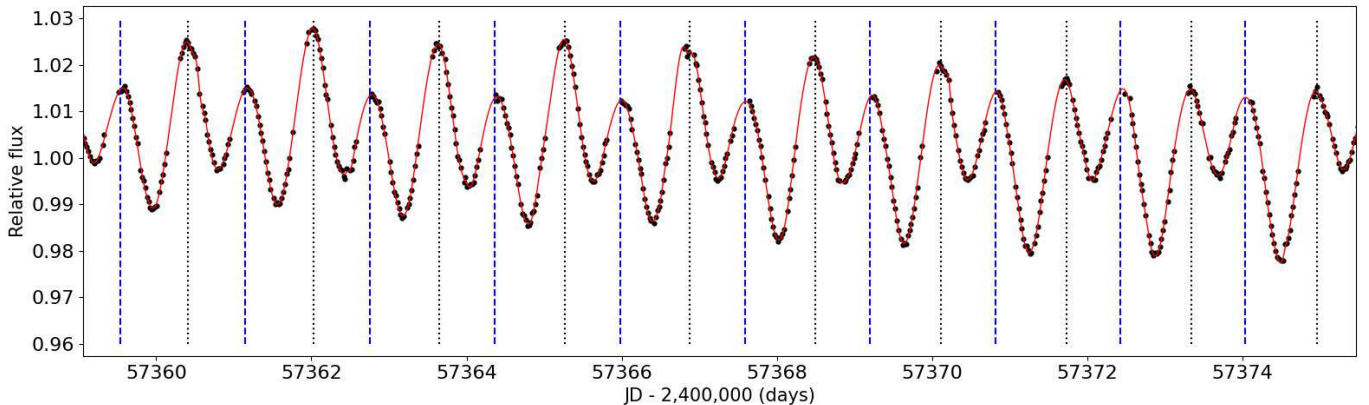


Figure 6. Section of the light curve of EPIC 219511354 showing the presence of two signals with slightly different periods. The red line is a spline fit to the data to guide the eye. Alternating peaks are marked with dotted and dashed lines, and have apparent periods of 1.617 and 1.612 days, respectively.

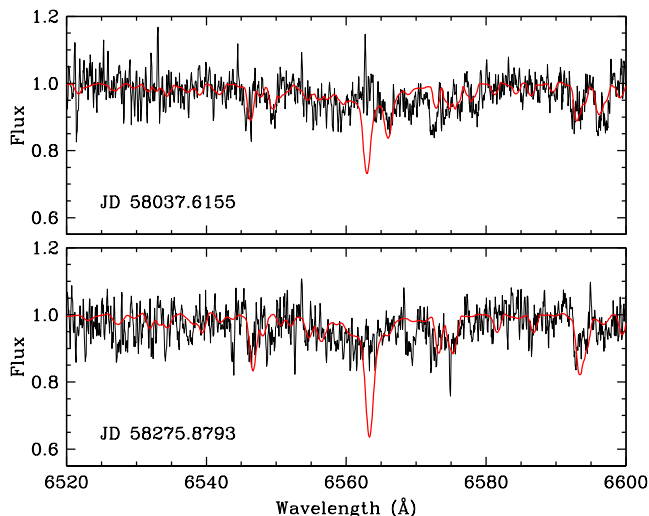


Figure 7. Two of our spectra for EPIC 219511354 in the $H\alpha$ region, compared against synthetic double-lined spectra (red lines) constructed from individual PHOENIX models for each component, Doppler shifted according to their measured velocities, and scaled in accordance with their flux ratio. Julian dates ($-2,400,000$) for the observations are indicated in each panel.

rotation. The primary star is about 40% brighter, but the secondary could well be more active, so the relative strengths of the signals may actually be similar. It seems likely, therefore, that both components are contributing to the variability out-of-eclipse.

Other common signatures of activity include the presence of emission cores in the Ca II H and K lines, and the $H\alpha$ line in emission. The flux in the blue part of our spectra is too low to detect the calcium lines, but the $H\alpha$ feature does suggest a modest level of activity. Figure 7 shows two of our best spectra in this region at different orbital phases, compared against double-lined synthetic spectra for the appropriate phases. We generated the synthetic spectra using PHOENIX models from Husser et al. (2013), for the temperatures and surface gravities of the two components and an estimated flux ratio of 0.64 at this wavelength. The $H\alpha$ line is missing, or perhaps slightly in emission in the top panel. At the very least the line appears to be completely filled in, which is evidence of chromospheric activity.

Finally, EPIC 219511354 has been detected in X-rays by the Swift mission (Evans et al. 2020), in observations

carried out between 2014 and 2018. This, and the other signs of activity, are driven by the tidally induced rapid rotation of the stars, which is more than an order of magnitude faster than single stars of this mass in the cluster (see Curtis et al. 2020).

6. COMPARISON WITH MODELS

Precisely measured masses, radii, and effective temperatures of stars in eclipsing binaries can provide important tests of stellar evolution theory, particularly when the masses and radii are determined to better than 3%, as is the case for EPIC 219511354 (see, e.g., Andersen 1991; Torres et al. 2010). In many of these comparisons with models the metallicity of the system and its age are often not known, and must be left as free parameters. This tends to weaken the test. Membership of EPIC 219511354 in Ruprecht 147 makes it an ideal case for such a comparison, because estimates are available for both of those properties. The metallicity is close to $[\text{Fe}/\text{H}] = +0.10$ (Curtis et al. 2018; Bragaglia et al. 2018), and our earlier studies in Papers I–III of three other eclipsing binaries in Ruprecht 147 have provided an age estimate for the cluster of 2.67 ± 0.21 Gyr, based on the PARSEC 1.2S models of Chen et al. (2014).

Figure 8 compares the measured properties of the EPIC 219511354 components with the same models as above, for the known metallicity and age of the parent cluster. Other eclipsing binaries from the literature with components that have masses and radii measured to 3% or better and are in the same mass range are shown as well. At the measured masses for EPIC 219511354, the radii of both components are significantly larger than predicted, by about 10% (5.3σ) for the primary and 14% (6.4σ) for the secondary. At the same time, the effective temperatures are seen to be cooler than predicted, by 310 K and 270 K, respectively, or roughly 6% (2σ).¹⁰ Both of these trends go in the same direction as observed in many other active lower main-sequence stars (e.g., Torres 2013), and point to the activity of EPIC 219511354 as the cause of the deviations from theory. The systematic deviations are usually referred to as

¹⁰ Note that the primary and secondary temperatures are strongly correlated, and that their difference is much better determined than their absolute values through the use of J_{ave} , as described earlier. The models predict a primary/secondary difference of 390 K, quite close to the measured value of 345 ± 60 K.

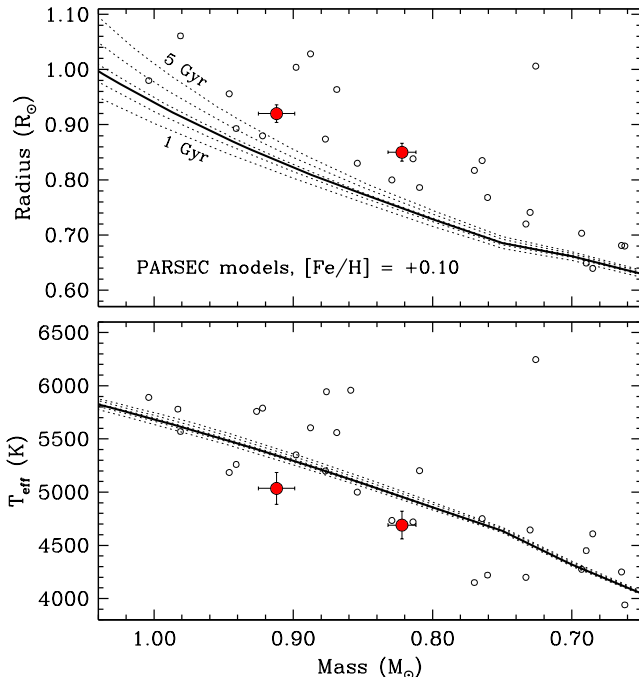


Figure 8. Comparison of the mass, radius, and effective temperature measurements for EPIC 219511354 against isochrones from the PARSEC 1.2S series of Chen et al. (2014), for the adopted metallicity of the Ruprecht 147 cluster, $[\text{Fe}/\text{H}] = +0.10$. The heavy line corresponds to the age of 2.67 Gyr determined from three previously studied eclipsing binaries in the cluster (Torres et al. 2018, 2019, 2020). Dotted lines represent isochrones from 1 to 5 Gyr from the same models. Masses, radii, and temperatures for other eclipsing binaries from the literature that are in the same mass regime as EPIC 219511354 and have fractional errors below 3% are shown for context.

“radius inflation” and “temperature suppression”.

On the other hand, the bolometric luminosities predicted by the models, $L_{\text{Aa}} = 0.51 L_{\odot}$ and $L_{\text{Ab}} = 0.31 L_{\odot}$, are in good agreement with our empirical estimates of 0.490 ± 0.060 and $0.316 \pm 0.038 L_{\odot}$ for the primary and secondary, respectively. This is a direct result of the Stefan-Boltzmann law, and the fact that the fractional radius discrepancies with the models are roughly twice as large as those in the temperatures.

It is worth noting that the PARSEC models we have used for this comparison differ from other standard models in that they have been modified by their builders in an attempt to “correct” the problems of radius inflation and temperature suppression. As explained by Chen et al. (2014), this was done by adjusting the temperature-opacity relation for stars less massive than about $0.7 M_{\odot}$ (at solar metallicity), in such a way as to increase the radii enough to match observations of low-mass stars in the mass-radius diagram. Both components of EPIC 219511354 are more massive than $0.7 M_{\odot}$, so those adjustments should not have an impact on them, and the PARSEC models effectively behave as standard models for these stars.

7. DISCUSSION AND FINAL REMARKS

It was our expectation at the beginning of this study that precise and accurate masses, radii, and effective temperatures for EPIC 219511354 would allow for a stringent test of stellar evolution models and an independent estimate of the age of Ruprecht 147, to supplement

similar determinations for three other eclipsing binaries in the cluster analyzed previously. While the significant level of activity in EPIC 219511354 has prevented us from doing that, it has rewarded us with a rare opportunity for an assumption-free estimate of the degree of radius inflation and temperature suppression, because of the fact that the metallicity and age of Ruprecht 147 are already known. This is not usually the case for a typical low-mass eclipsing binary in the field. The radius and temperature deviations from theory in those cases are often measured with reference to an arbitrary isochrone of solar metallicity and some fixed age that varies from author to author, so they depend to some extent on those assumptions. Age may well have a relatively small effect, especially for M dwarfs, but that is not the case for the metallicity (see, e.g., Berger et al. 2006).

Stellar activity such as we see in EPIC 219511354 is typically associated with strong magnetic fields and/or the presence of spots. Magnetic fields tend to inhibit convection and slow the outward transport of energy (e.g., Chabrier et al. 2007), and the stars adjust by increasing their surface area and reducing their surface temperature. Star spots are thought to elicit a similar response (Chabrier et al. 2007; Somers & Pinsonneault 2015). Although most publicly available “standard” models of stellar evolution do not account for these effects, a few efforts in this direction to include non-standard physics have been made, with promising results (e.g., D’Antona et al. 2000; MacDonald & Mullan 2009, 2014; Feiden & Chaboyer 2013, 2014; Somers & Pinsonneault 2015; Somers et al. 2020). Of the small number of detailed comparisons of eclipsing binary observations against these non-standard models that have been made, almost all have involved active M dwarfs. One exception is the F+K system EF Aqr (Feiden & Chaboyer 2012). EPIC 219511354 therefore represents an ideal case to test those models for a pair of K dwarfs with absolute masses, radii, and temperatures measured to better than 3%, and a known age and metallicity.

Turning now to the multiplicity of EPIC 219511354, it is interesting to note that this is the second hierarchical triple system found among the four eclipsing binaries in Ruprecht 147 that we have studied thus far. This is not surprising given its 1.6 day orbital period, as Tokovinin et al. (2006) have shown that the vast majority ($\sim 96\%$) of spectroscopic binaries with periods under 3 days have additional components. The other triple system we have found is EPIC 219552514 (Torres et al. 2020), with a period of 2.75 days.¹¹

As was the case in that system, the nature of the third star in the present one is unclear. If it is a lower main-sequence star, we have estimated its mass to be in the range $0.27\text{--}0.47 M_{\odot}$, corresponding to a mid-to-late M dwarf. If a white dwarf, it could be more massive. In either case, the third star may affect the dynamical evolution of the system. For example, it could modulate the angle between the inner and outer orbital planes through Kozai-Lidov oscillations (e.g., Naoz 2016), as well as the eccentricity of the inner eclipsing system. We have, in fact, found some evidence, tentative as it may be, that

¹¹ The remaining two eclipsing binaries, EPIC 219394517 and EPIC 219568666 (Torres et al. 2018, 2019), have longer periods of 6.53 and 11.99 days, and are not known to have third components.

the inner orbit may be slightly eccentric, whereas given the present age of the system it would be expected to have long been circularized (on a timescale of ~ 10 Myr; e.g., Hilditch 2001). Confirmation of this non-zero eccentricity must await new observations, preferably high-precision light curves that are more sensitive to the eccentricity. Current observing plans for NASA’s TESS mission do not include pointings near EPIC 219511354 for the near future. Based on the dynamical stability criteria of Eggleton & Kiseleva (1995) and Mardling & Aarseth (2001), we find that for any reasonable mass of the third star and any relative inclination of the orbital planes, the EPIC 219511354 system is in no danger of being disrupted.

The angular size of the outer orbit is estimated to be about 3 mas. While this would be within reach of long-baseline interferometers such as CHARA, VLTI, or NPOI, the system is likely too faint for the sensitivity of current instrumentation ($V = 13.0$, $K = 10.6$). The Gaia mission cannot spatially resolve the third star, but could in principle detect the wobble of the center of light of the system. The renormalized unit weight error (RUWE) from the Gaia EDR3 catalog, which is indicative of the quality of the astrometric solution, has a value for EPIC 219511354 of 1.183. This is nominally within the range of 1.0–1.4 in which the solutions are considered acceptable¹², although Stassun & Torres (2021) have reported based on a large sample of eclipsing binaries that even within that range the RUWE values tend to correlate with the semimajor axis of the motion of the photocenter. Another useful indicator of a perturbed astrometric solution is the `astrometric_excess_noise` parameter, for which Gaia gives the value 0.09 mas. The statistical significance attached to this quantity is $D = 5.23$ (a dimensionless measure of significance). Values larger than about $D = 2.0$ are regarded as a sign that there may be unmodeled motion in the source. It is possible, therefore, that Gaia has already detected the signature of the triple system. If confirmed, this could eventually yield the inclination angle of the outer orbit, which would then enable the mass of the tertiary to be determined, perhaps clarifying its true nature.

The spectroscopic observations of EPIC 219511354 were gathered with the help of P. Berlind, M. Calkins, and G. Esquerdo. J. Mink is thanked for maintaining the CfA echelle database. We thank the anonymous referee for helpful comments. G.T. acknowledges partial support from NASA’s Astrophysics Data Analysis Program through grant 80NSSC18K0413. J.L.C. is supported by the NSF Astronomy and Astrophysics Postdoctoral Fellowship under award AST-1602662, and by NASA under grant NNX16AE64G issued through the K2 Guest Observer Program (GO 7035). E.G. acknowledges support from NSF Astronomy & Astrophysics grant 1817215. The research has made use of the SIMBAD and VizieR databases, operated at the CDS, Strasbourg, France, and of NASA’s Astrophysics Data System Abstract Service. The work has also made use of data from the European Space Agency (ESA) mission Gaia (<https://www.cosmos.esa.int/gaia>), pro-

cessed by the Gaia Data Processing and Analysis Consortium (DPAC, <https://www.cosmos.esa.int/web/gaia/dpac/consortium>). Funding for the DPAC has been provided by national institutions, in particular the institutions participating in the Gaia Multilateral Agreement. The computational resources used for this research include the Smithsonian Institution’s “Hydra” High Performance Cluster.

REFERENCES

- Andersen, J. 1991, *A&A Rev.*, 3, 91
- Andersen, J., Clausen, J. V., & Nordstrom, B. 1980, in *IAU Symp. 88, Close Binary Stars: Observations and Interpretation*, eds. M. J. Plavec, D. M. Popper & R. K. Ulrich (Dordrecht, The Netherlands: Reidel), 81
- Berger, D. H., Gies, D. R., McAlister, H. A., et al. 2006, *ApJ*, 644, 475
- Binnendijk, L. 1960, *Properties of Double Stars*, (Univ. of Pennsylvania Press: Philadelphia), p. 290
- Bragaglia, A., Fu, X., Mucciarelli, A., Andreuzzi, G., & Donati, P. 2018, *A&A*, 619, A176
- Casagrande, L., Ramírez, I., Meléndez, J., Bessell, M., & Asplund, M. 2010, *A&A*, 512, A54
- Chabrier, G., Gallardo, J., & Baraffe, I. 2007, *A&A*, 472, L17
- Chen, Y., Girardi, L., Bressan, A., et al. 2014, *MNRAS*, 444, 2525
- Claret, A., & Bloemen, S. 2011, *A&A*, 529, A75
- Curtis, J. L. 2016, PhD Thesis, Penn State University
- Curtis, J. L., Agüeros, M. A., Matt, S. P., et al. 2020, *ApJ*, 904, 140
- Curtis, J. L., Vanderburg, A., Torres, G., et al. 2018, *AJ*, 155, 173
- Curtis, J. L., Wolfgang, A., Wright, J. T., Brewer, J. M., & Johnson, J. A. 2013, *AJ*, 145, 134
- D’Antona, F., Ventura, P., & Mazzitelli, I. 2000, *ApJ*, 543, L77
- Eggleton, P., & Kiseleva, L. 1995, *ApJ*, 455, 640
- Etzel, P. B. 1981, *Photometric and Spectroscopic Binary Systems*, Proc. NATO Adv. Study Inst., ed. E. B. Carling & Z. Kopal (Dordrecht: Reidel), p. 111
- Evans, P. A., Page, K. L., Osborne, J. P., et al. 2020, *ApJS*, 247, 54
- Feiden, G. A. & Chaboyer, B. 2012, *ApJ*, 761, 30
- Feiden, G. A., & Chaboyer, B. 2013, *ApJ*, 779, 183
- Feiden, G. A., & Chaboyer, B. 2014, *ApJ*, 789, 53
- Flower, P. J. 1996, *ApJ*, 469, 355
- Foreman-Mackey, D., Hogg, D. W., Lang, D., & Goodman, J. 2013, *PASP*, 125, 306
- Fűrész, G. 2008, PhD thesis, Univ. Szeged, Hungary
- Gaia Collaboration, Brown, A. G. A., Vallenari, A., et al. 2021, *A&A*, 649, A1
- Gelman, A., & Rubin, D. B. 1992, *Statistical Science*, 7, 457
- Gilliland, R. L. 1986, *ApJ*, 300, 339
- Gilliland, R. L., Jenkins, J. M., Borucki, W. J., et al. 2010, *ApJ*, 713, L160
- Goodman, J., & Weare, J. 2010, *Commun. Appl. Math. Comput. Sci.*, 5, 65
- Henden, A. A., Levine, S., Terrell, D., & Welch, D. L. 2015, *American Astronomical Society Meeting Abstracts #225*, 225, 336.16
- Hilditch, R. W. 2001, *An Introduction to Close Binary Stars* (Cambridge, UK: Cambridge University Press) p. 152
- Hora, J. L., Luppini, G. A., & Hodapp, K.-W. 1994, *Proc. SPIE*, 2198, 498
- Huang, Y., Liu, X.-W., Yuan, H.-B., et al. 2015, *MNRAS*, 454, 2863
- Husser, T.-O., Wende-von Berg, S., Dreizler, S., et al. 2013, *A&A*, 553, A6
- Irwin, J. M., Quinn, S. N., Berta, Z. K., et al. 2011, *ApJ*, 742, 123
- Kipping, D. M. 2010, *MNRAS*, 408, 1758
- Kraus, A. L., Ireland, M. J., Huber, D., Mann, A. W., & Dupuy, T. J. 2016, *AJ*, 152, 8
- Latham, D. W., Stefanik, R. P., Torres, G., et al. 2002, *AJ*, 124, 1144
- Lindgren, L., Bastian, U., Biermann, M., et al. 2021, *A&A*, 649, A4
- MacDonald, J., & Mullan, D. J. 2009, *ApJ*, 700, 387

¹² See report by L. Lindgren in the Gaia documentation, <https://www.cosmos.esa.int/web/gaia/public-dpac-documents>

- MacDonald, J., & Mullan, D. J. 2014, *ApJ*, 787, 70
- Mardling, R. A., & Aarseth, S. J. 2001, *MNRAS*, 321, 398
- Marigo, P., Cummings, J. D., Curtis, J. L., et al. 2020, *Nature Astronomy*, 4, 1102.
- Naoz, S. 2016, *ARA&A*, 54, 441
- Nordström, B., Latham, D. W., Morse, J. A., et al. 1994, *A&A*, 287, 338
- Pevtsov, A. A., Fisher, G. H., Acton, L. W. et al. 2003, *ApJ*, 598, 1387
- Popper, D. M., & Etzel, P. B. 1981, *AJ*, 86, 102
- Prša, A., Harmanec, P., Torres, G., et al. 2016, *AJ*, 152, 41
- Reiners, A. 2012, *Living Reviews in Solar Physics*, 9, 1
- Saar, S. H. 2001, 11th Cambridge Workshop on Cool Stars, Stellar Systems and the Sun, ASP Conv. Ser., 223, eds. R. J. García López, R. Rebolo and M. R. Zapatero Osorio (San Francisco: ASP), 292
- Skrutskie, M. F., Cutri, R. M., Stiening, R., et al. 2006, *AJ*, 131, 1163
- Somers, G., & Pinsonneault, M. H. 2015, *ApJ*, 807, 174
- Somers, G., Cao, L., & Pinsonneault, M. H. 2020, *ApJ*, 891, 29
- Stassun, K. G. & Torres, G. 2021, *ApJ*, 907, L33
- Szentgyorgyi, A. H., & Fűrész, G. 2007, *Precision Radial Velocities for the Kepler Era*, in The 3rd Mexico-Korea Conference on Astrophysics: Telescopes of the Future and San Pedro Mártir, ed. S. Kurtz, RMxAC, 28, 129
- Tokovinin, A., Thomas, S., Sterzik, M., et al. 2006, *A&A*, 450, 681
- Torres, G. 2010, *AJ*, 140, 1158
- Torres, G. 2013, *Astronomische Nachrichten*, 334, 4
- Torres, G., Andersen, J., & Giménez, A. 2010, *A&A Rev.*, 18, 67
- Torres, G., Curtis, J. L., Vanderburg, A., Kraus, A. L., & Rizzuto, A. 2018, *ApJ*, 866, 67 (Paper I)
- Torres, G., Latham, D. W., & Stefanik, R. P. 2007, *ApJ*, 662, 602
- Torres, G., Neuhäuser, R., & Guenther, E. W. 2002, *AJ*, 123, 1701
- Torres, G., Vanderburg, A., Curtis, J. L., et al. 2019, *ApJ*, 887, 109 (Paper II)
- Torres, G., Vanderburg, A., Curtis, J. L., et al. 2020, *ApJ*, 896, 162 (Paper III)
- Vanderburg, A., & Johnson, J. A. 2014, *PASP*, 126, 948
- Vanderburg, A., Latham, D. W., Buchhave, L. A., et al. 2016, *ApJS*, 222, 14
- Wright, N. J., Newton, E. R., Williams, P. K. G., et al. 2018, *MNRAS*, 479, 2351
- Zucker, S., & Mazeh, T. 1994, *ApJ*, 420, 806
- Zucker, S., Torres, G., & Mazeh, T. 1995, *ApJ*, 452, 863